ZANCO Journal of Pure and Applied Sciences

TYPE Original article
DOI http://dx.doi.org/10.21271/ZJPAS.38.3.3

OPEN ACCESS

*Corresponding author
Othman Q. Ahmed
othman.qadir@uor.edu.krd

RECEIVED :09 /08/2025
ACCEPTED :03/11/ 2025
PUBLISHED :30/06/ 2026

KEYWORDS:
Lü system, Hopf bifurcation, First Lyapunov coefficient, Poincaré compactification.

Dynamic Analysis and Hopf Bifurcation of a Modified Lü System

Rizgar H. Salih & Othman Q. Ahmed*
Department of Mathematics, Collage of Basic Education, University of Raparin, Rania, Kurdistan Region, Iraq

ABSTRACT

The stability and Hopf bifurcation of a modified Lü system are investigated, with a focus on the conditions that lead to the emergence of periodic solutions. The criteria for Hopf bifurcations at non-origin equilibrium points are established and the stability of the resulting periodic solutions is analyzed using the first Lyapunov coefficient. A detailed exploration of the system's dynamics reveals both stable and unstable periodic solutions, depending on parameter values. Numerical examples are provided to illustrate these findings, underscoring the critical role of parameters in determining the nature of bifurcating periodic solutions. Additionally, Poincaré compactification theory is employed to analyze the system's behavior at infinity, providing insights into its global dynamics and enhancing the understanding of the modified Lü system's complex behavior.

1.Introduction

Chaotic systems represent one of the most fascinating and significant phenomena in nonlinear dynamics, having garnered extensive research attention over recent decades due to their complex dynamical behavior and practical utility in various applications, including engineering systems, power grid dynamics and secure communication technologies (*Chen and Dong, 1998*, *Lü et al., 2002b*). The intricate nature of chaos, characterized by sensitive dependence on initial conditions and aperiodic long-term behavior, has made it a cornerstone of modern nonlinear science.

Among the classic chaotic systems, the Lorenz system, introduced by Lorenz in 1963 (*Lorenz, 1963*, *Lorenz, 2017*), stands as the first well-known chaotic attractor a third-order autonomous system with two nonlinear multiplicative terms exhibiting intricate dynamical behavior. Subsequently, Chen and collaborators discovered another chaotic attractor in 1999 (*Chen and Ueta, 1999*, *Ueta and Chen, 2000*) that, while structurally similar, is not mathematically equivalent to the Lorenz system. More recently, Lü and Chen identified a new chaotic system that bridges the gap between the Lorenz and Chen systems (*Lü and Chen, 2002*), described by:

$$\dot{x} = -a(x-y), \quad \dot{y} = -xz + cy, \quad \dot{z} = xy - bz, \quad (1)$$

where a, b and c are constant parameters. These three systems can be distinguished by analyzing their structural characteristics when decomposed into linear and nonlinear components in the form $Ax + f(x)$, where $A = [a_{ij}]$: the Lorenz system satisfies $a_{12}a_{21} > 0$, the Chen system satisfies $a_{12}a_{21} < 0$ and the Lü system meets the condition $a_{12}a_{21} = 0$ (*Vaněček and Čelikovský, 1996*).

Extensive research has been conducted on the classical Lü system, analyzing its local and global dynamical behaviors, chaotic characteristics, routes to chaos, feedback control strategies, invariant algebraic surfaces and synchronization properties. Lü, Chen and Zhang explored the fundamental characteristics, bifurcation patterns and paths to chaos of the newly proposed chaotic attractor using analytical and numerical methods (*Lü et al., 2002a*). Yu and Zhang examined the stability and bifurcation of the Lü system, deriving conditions for supercritical and subcritical bifurcations (*Yu and Zhang, 2003*) and later analyzed the Hopf bifurcation while proposing practical methods for distinguishing between chaotic, periodic and quasi-periodic orbits (*Yu and Zhang, 2004*). Mello and Coelho proposed that the non-origin equilibrium points are centers under specific parameter conditions ($b = 2c$, $a = c$ and $ab > 0$) (*Mello and Coelho, 2009*), which was validated by Buică et al. through identifying a global inverse Jacobi multiplier (*Buică et al., 2012*). Salih and Hasso demonstrated that under these criteria, only one periodic solution can bifurcate from each non-origin equilibrium point (*Salih and Hasso, 2017*).

Several modifications of the Lü system have been proposed to explore extended dynamical behaviors. Wang, Zhang, Zheng and Li introduced a modified version in 2006 by adding a cross-product term to the first equation (*Wang et al., 2006*):

$$\dot{x} = a(y - x + yz), \quad \dot{y} = -xz + by, \quad \dot{z} = xy - cz, \quad (2)$$

Xiao and Cao focused on controlling the Lü chaotic attractor by introducing time-delayed feedback (*Xiao and Cao, 2007*), while Huang and Cao modified the system by replacing the term xy in the third equation with e^{xy} (*Huang and Cao, 2014*). Jiang and Wu proposed another modification by adding parameters to create the system (*Jiang and Wu, 2016*):

$$\dot{x} = -a(x - y^2), \quad \dot{y} = by - cz, \quad \dot{z} = gxy - dz, \quad (3)$$

where a, b, c, d and g are constant parameters.

Current research on stability and bifurcation analysis in chaotic systems has revealed the fundamental importance of Hopf bifurcation, which has become a widely studied topic (*Dias and Mello, 2013*, *Guo et al., 2023*, *Sun et al., 2006*, *Llibre and Pessoa, 2015*, *Wang, 2009*, *Van Gorder and Choudhury, 2011*, *Wu and Fang, 2015*). This bifurcation involves the creation or disappearance of periodic solutions around an equilibrium point and can be supercritical or subcritical (*Strogatz, 2024*). What distinguishes Hopf bifurcation from other bifurcations, such as saddle-node or pitchfork bifurcations, are two key features: it requires at least two dimensions and involves the appearance or disappearance of periodic solutions. Various analytical methods, including bifurcation formulas (*Sotomayor et al., 2006*, *Sotomayor et al., 2007*, *Sarmah et al., 2015*, *Mohammed, 2024*), Lyapunov coefficients (*Salih, 2015*, *Salih and Mohammed, 2022*, *Rasul and Salih, 2024*) and focus quantities (*Sang and Huang, 2017*, *Sang, 2021*), have been developed to study these phenomena.

Despite extensive research on various modifications of the Lü system, significant gaps remain in the literature regarding the comprehensive analysis of periodic solutions and their stability characteristics in modified Lü systems. Specifically, there is limited understanding of how parameter variations affect the nature of bifurcating periodic solutions in system (3) and the global dynamical behavior near infinity has not been thoroughly investigated using modern analytical techniques.

Understanding the stability and Hopf bifurcation characteristics of this modified system is crucial for several reasons. First, analyzing Hopf bifurcation is essential for understanding the stability of periodic orbits, making it a key aspect of bifurcation theory (*Sotomayor et al., 2006*, *Algaba et al., 2015*, *Blé et al., 2016*). Second, the study of periodic solutions provides fundamental insights into the transition between different dynamical regimes, which is vital for predicting and controlling system behavior. Third, the stability analysis of bifurcating periodic solutions using the first Lyapunov coefficient offers precise mathematical tools for determining whether emerging periodic solutions are stable or unstable, thereby providing a complete characterization of local dynamics around equilibrium points.

This study presents comprehensive analytical and numerical findings regarding the periodic solutions of the modified Lü system (3) through Hopf bifurcation analysis. We establish the conditions for the occurrence of Hopf bifurcations at non-origin equilibrium points and analyze the stability of the resulting periodic solutions using the first Lyapunov coefficient. Our investigation reveals both stable and unstable periodic solutions depending on parameter values, with numerical examples demonstrating the critical role of parameters in determining the nature of bifurcating periodic solutions. Furthermore, we employ Poincaré compactification theory to analyze the system's behavior at infinity, providing insights into global dynamics.

The practical implications of this research extend to various fields where chaotic systems find applications. Understanding the conditions for periodic solution emergence and their stability characteristics can inform the design of control strategies in engineering systems, contribute to the development of secure communication protocols based on chaotic synchronization and provide theoretical foundations for applications in power grid dynamics where periodic behavior may be either desired or avoided.

The remainder of this paper is organized as follows: Section 2 addresses the determination of equilibrium points of system (3) and analyzes their stability properties. Section 3 explores the Hopf bifurcation, including the conditions under which it occurs, as well as the stability and direction of resulting periodic solutions using the Center Manifold theorem. Section 4 examines the system's behavior near and at infinity using Poincaré compactification. Finally, Section 5 concludes with a summary of the main finding.

2 Stability Analysis of Equilibrium points

Equilibrium points are considered the basic foundation for understanding the different aspects of any dynamical system. By solving $-a(x-y^2)=by-cz=gxy-dz=0$, the following three equilibrium points of system (3) are obtained: $E_0(0.0.0)$ and $E_{1.2}\left(x_0,\pm\sqrt{x_0},\pm\frac{b}{c}\sqrt{x_0}\right)$, where $x_0=\frac{bd}{cg}$ and $bcdg>0$. It should be noted that $E_{1,2}$ represents the pairs of symmetric equilibria and only one, which is E_1, will be analyzed.

Proposition 1. *The stability of the equilibrium point E_0 can be evaluated based on the following conditions:*

1. *If $a>0, d>0$ and $b<0$, then E_0 is asymptotically stable.*
2. *If $abd>0$, then E_0 is unstable.*

3. *If $d = 0, a > 0$ and $b < 0$, then E_0 is asymptotically stable when $cg > 0$ and E_0 is unstable when $cg < 0$.*
4. *If $b = 0, a > 0$ and $d > 0$, then E_0 is asymptotically stable if $cg > 0$ and E_0 is unstable if $cg < 0$.*

Proof. The Jacobian matrix of system (3) at E_0 is given by:

$$J = \begin{pmatrix} -a & 0 & 0 \\ 0 & b & -c \\ 0 & 0 & -d \end{pmatrix} \qquad (4)$$

and it has the following eigenvalues: $\lambda_1 = -a, \lambda_2 = b$ and $\lambda_3 = -d$.

1. When $a > 0$, $d > 0$ and $b < 0$, the eigenvalues of the Jacobian matrix (4) are negative. Therefor, E_0 is asymptotically stable (see Fig. 1-(a)).

2. When $abd > 0$ then the determinant of the jacobian matrix (4) is positive. This implies that at least one of the eigenvalues is positive. Therefor E_0 is unstable (see Fig. 1-(b,c,d)).

3. When $d = 0$, the eigenvalues of (4) are $\lambda_1 = -a, \lambda_2 = b$ and $\lambda_3 = 0$, so the point E_0 is a non-hyperbolic equilibrium point. We transform system (3) into the canonical form using the following linear transformation so as to apply the center manifold theorem.

$$\begin{pmatrix} x \\ y \\ z \end{pmatrix} = M \begin{pmatrix} u \\ v \\ w \end{pmatrix}, \text{where } M = \begin{pmatrix} 0 & 1 & 0 \\ \frac{c}{b} & 0 & 1 \\ 1 & 0 & 0 \end{pmatrix}.$$

Thus, system (3) becomes:

$$\begin{pmatrix} \dot{u} \\ \dot{v} \\ \dot{w} \end{pmatrix} = \begin{pmatrix} 0 \\ -av \\ bw \end{pmatrix} + \begin{pmatrix} \frac{cg}{b} uv + gvw \\ \frac{ac^2}{b^2} u^2 + \frac{2ac}{b} uw + aw^2 \\ -\frac{c^2 g}{b^2} uv - \frac{cg}{b} vw \end{pmatrix}. \quad (5)$$

One dimensional local center manifold of system (5) near origin is the following set.
$W^c_{loc}(E_0) = \{ (u, v, w) \in \mathbb{R}^3 : v = h_1(u), w = h_2(u), h_1(0) = h_1'(0) = h_2(0) = h_2'(0) = 0\}$.
From Taylor expansion near the origin, $h_1(u) = a_1 u^2 + O(u^3)$ and $h_2(u) = b_1 u^2 + O(u^3)$. Substituting $v = h_1(u)$ and $w = h_2(u)$, we have that

$$h_1'(u)\dot{u} = \dot{v}$$

$$\left(2a_1 u + O(u^2)\right)\left(\frac{cg}{b} u h_1(u) + g h_1(u) h_2(u)\right) = -a h_1(u) + \frac{ac^2}{b^2} u^2 + \frac{2ac}{b} u h_2(u) + a\left(h_2(u)\right)^2$$

and

$$h_2'(u)\dot{u} = \dot{w}$$

$$\left(2b_1 u + O(u^2)\right)\left(\frac{cg}{b} u h_1(u) + g h_1(u) h_2(u)\right) = b h_2(u) - \frac{gc^2}{b^2} u h_1(u) - \frac{cg}{b} h_1(u) h_2(u).$$

In the system equating the coefficient of u^2 on both sides, then $a_1 = \frac{c^2}{b^2}$, $b_1 = 0$.
Consequently,

$$h_1(u) = \frac{c^2}{b^2} u^2 + O(u^3) \text{ and } h_2(u) = O(u^3).$$

The vector field is restricted to the center manifold which is given by

$$\dot{u} = \frac{gc^3}{b^3} u^3 + O(u^4). \qquad (6)$$

- When $cg > 0$, then $\frac{c^3 g}{b^3}$ is negative and $u = 0$ is asymptotically stable for equation (6). Thus, we obtain $(u, v, w) = (0,0,0)$ is asymptotically stable for system (5), so E_0 is asymptotically stable for system (3) (see Fig. 1-(e)).

- When $cg < 0$, then $\frac{gc^3}{b^3}$ is positive and $u = 0$ is unstable for equation (6). Thus, we obtain $(u, v, w) = (0,0,0)$ is unstable for system (5), so E_0 is unstable for system (3) (see Fig. 1-(f)).

4. When $b = 0$, the eigenvalues of (4) are $\lambda_1 = -a$, $\lambda_2 = 0$ and $\lambda_3 = -d$, so the point E_0 is a non-hyperbolic equilibrium point. We transform the system (3) into the canonical form using the following linear transformation to apply the center manifold theorem.

$$\begin{pmatrix} x \\ y \\ z \end{pmatrix} = M \begin{pmatrix} u \\ v \\ w \end{pmatrix}, \text{ where } M = \begin{pmatrix} 0 & 1 & 0 \\ 1 & 0 & \frac{c}{d} \\ 0 & 0 & 1 \end{pmatrix}.$$

Thus, system (3) becomes:

$$\begin{pmatrix} \dot{u} \\ \dot{v} \\ \dot{w} \end{pmatrix} = \begin{pmatrix} 0 \\ -av \\ -dw \end{pmatrix} + \begin{pmatrix} -\frac{cg}{d} uv - \frac{c^2 g}{d^2} vw \\ au^2 + \frac{2ac}{d} uw + \frac{ac^2}{d^2} w^2 \\ guv - \frac{cg}{d} vw \end{pmatrix}. \quad (7)$$

One dimensional local center manifold of system (7) near origin is the following set.

$$W^c_{loc}(E_0) = \{ (u, v, w) \in \mathbb{R}^3 : v = h_1(u), w = h_2(u), h_1(0) = h_1'(0) = h_2(0) = h_2'(0) = 0\}.$$

From Taylor expansion near the origin, $h_1(u) = a_1 u^2 + O(u^3)$ and $h_2(u) = b_1 u^2 + O(u^3)$. Substituting $v = h_1(u)$ and $w = h_2(u)$, we have that

$$h_1'(u)\dot{u} = \dot{v}$$

$$\left(2a_1 u + O(u^2)\right)\left(-\frac{cg}{d} u h_1(u) - \frac{c^2 g}{d^2} h_1(u) h_2(u)\right) = -a h_1(u) + au^2 + \frac{2ac}{d} u h_2(u) + \frac{ac^2}{d^2}\left(h_2(u)\right)^2$$

and

$$h_2'(u)\dot{u} = \dot{w}$$

$$\left(2b_1 u + O(u^2)\right)\left(-\frac{cg}{d} u h_1(u) - \frac{c^2 g}{d^2} h_1(u) h_2(u)\right) = -d h_2(u) + gu h_1(u) + \frac{cg}{d} h_1(u) h_2(u).$$

In the system equating the coefficient of u^2 on both sides, then $a_1 = 1$, $b_1 = 0$. Consequently,

$$h_1(u) = u^2 + O(u^3) \text{ and } h_2(u) = O(u^3).$$

The vector field is restricted to the center manifold which is given by

$$\dot{u} = -\frac{cg}{d} u^3 + O(u^4). \quad (8)$$

- When $cg > 0$, then $u = 0$ is asymptotically stable for equation (8). Thus, we obtain $(u, v, w) = (0,0,0)$ is asymptotically stable for system (7), so E_0 is asymptotically stable for system (3) (see Fig. 1-(g)).

- When $cg < 0$, then $u = 0$ is unstable for equation (8). Thus, we find that $(u, v, w) = (0,0,0)$ is unstable for system (7), so E_0 is unstable for system (3) (see Fig. 1-(h)).

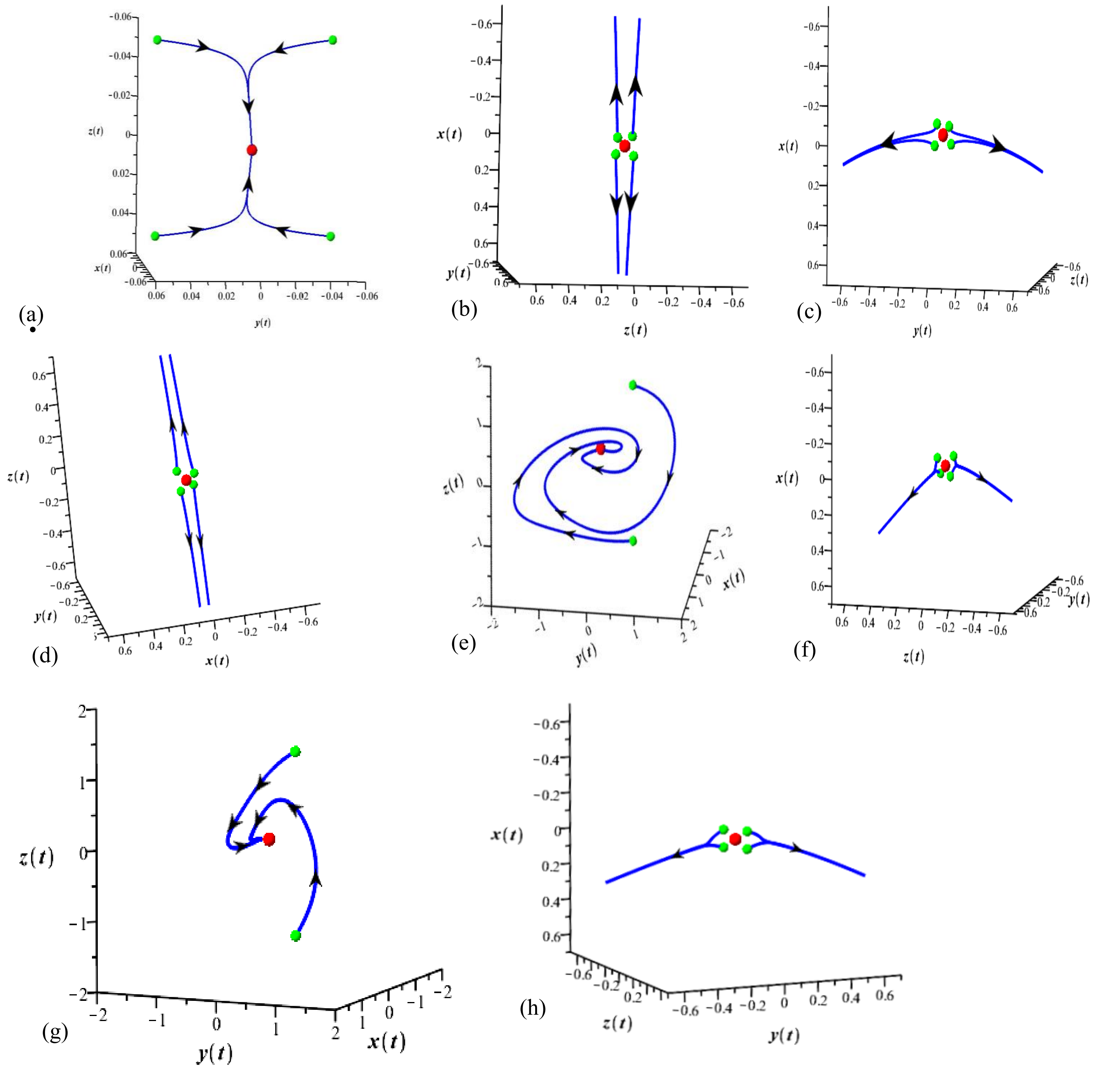

Figure 1: The phase portrait of system (3) in the neighborhood of the origin equilibrium point, E_0, is presented for the following cases: **(a)** $a = 0.1$, $b = -1$, $c = g = 0$, $d = 0.1$; **(b)** $a = b = -1$, $c = g = 1$, $d = 0.001$; **(c)** $a = b = c = d = g = 1$; **(d)** $a = 0.2$, $b = d = -1$, $c = g = 1$; **(e)** $a = 1$, $b = g = -1$, $c = -3$, $d = 0$; **(f)** $a = g = 1$, $b = -1$, $c = -3$, $d = 0$; **(g)** $b = 0$, $a = c = d = g = 1$; **(h)** $a = d = 1$, $b = 0$, $c = -3$, $g = 3$. The green balls, the red ball and the blue curves indicate the initial points, the equilibrium point and the trajectory, respectively. □

Proposition 2. *For the equilibrium point E_1, the following statements are asserted:*

5. *If $abd > 0$, $b < a + d$ and $a(ab - ad - b^2 + 4bd - d^2) < 0$, then E_1 is asymptotically stable.*
6. *If $abd < 0$, then E_1 is indicated to be unstable.*

Proof. The characteristic equation corresponding to the Jacobian matrix of system (3) at the equilibrium point E_1 is given by

$$\lambda^3 - T\lambda^2 - K\lambda - D = 0 \tag{9}$$

where $T = -a + b - d$, $K = -ad + ab$ and $D = -2abd$.

- It is indicated by Hurwitz's theorem that the equilibrium point E_1 is asymptotically stable if and only if $T < 0$, $D < 0$ and $TK + D > 0$ (Arrowsmith and Place, 1982). Thus, E_1 is asymptotically stable if and only if $b < a + d$, $abd > 0$ and $a(ab - ad - b^2 + 4bd - d^2) < 0$, (see Fig. 2-(a)).
- When $abd < 0$, it is concluded that the determinant, D, is positive and at least one of the roots of equation (9) is positive, indicating that the equilibrium point E_1 is unstable, (see Fig. 2-(b)).

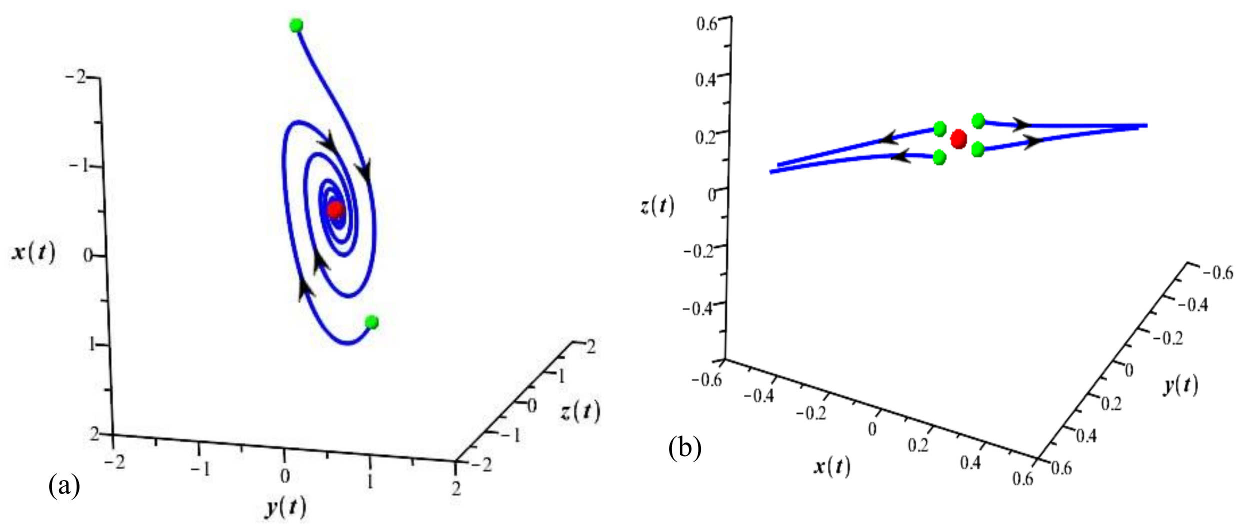

Figure 2: The phase portrait of system (3) in the neighborhood of the equilibrium point E_1 is presented for the following cases: **(a)** $a = 1$, $b = 0.5$, $c = 2, g = -1$, $d = -1$; **(b)** $a = -1$, $b = c = d = g = 1$. The green balls, the red ball and the blue curves indicate the initial points, the equilibrium point and the trajectories, respectively.

The findings presented in this section are summarized in Table 1.

Equilibrium	Conditions	Stability
E_0	$a > 0, d > 0, b < 0$	Asymptotically stable
E_0	$abd > 0$	Unstable
E_0	$d = 0, a > 0, b < 0$	Asymptotically stable if $gc^3 > 0$ Unstable if $gc^3 < 0$
E_0	$b = 0, a > 0, d > 0$	Asymptotically stable if $cg > 0$ Unstable if $cg < 0$
E_1	$abd > 0, b < a + d,$ $a(ab - ad - b^2 + 4bd - d^2) < 0$	Asymptotically stable
E_1	$abd < 0$	Unstable

3 Hopf Bifurcation

This section presents a discussion of the Hopf bifurcation that occurs in system (3) at the equilibrium point E_1. The direction and stability of the resulting periodic solutions, as well as the type of Hopf bifurcation, are explained using the Center Manifold Theorem as outlined in (*Guckenheimer and Holmes, 2013*). For more detailed information about this topic, see (*Amen and Salih, 2008*, *Algaba et al., 2015*, *Sarmah et al., 2015*, *Mikaeel et al., 2025*, *Mohammed, 2025*, *Salih, 2011*, *Husien and Amen, 2024*). For convenience, we define the following set of parameters:

$$\Omega_1 = \{ \quad (a,b,c,d,g) \in \mathbb{R}^5 : a = a^* = \frac{\omega^2}{d-b},\ bcdg > 0,\ b \neq d,\ \sigma_1 = \omega^4 - 2bd\big(6bd - (b^2+d^2)\big) \neq 0;$$
$$\omega = \sqrt{4bd - (b^2+d^2)}\ ,\ \omega > 0 \text{ and } \alpha = \frac{\omega^2(b-d)^2}{2\sigma_1}\}$$

The occurrence of the main result regarding the Hopf bifurcation is provided in the following proposition.

Proposition 3. *We consider $(a,b,c,d,g) \in \Omega_1$, then system (3) undergoes a Hopf bifurcation at the equilibrium point $E_1 = \left(x_0, \sqrt{x_0}, \frac{b}{c}\sqrt{x_0}\right)$.*

Proof. Suppose $(a,b,c,d,g) \in \Omega_1$. When $a = a^*$, equation (9) can be rewritten as

$$\frac{(\lambda(d-b)+2bd)(b^2-4bd+d^2-\lambda^2)}{b-d} = 0.$$

It is clear that equation (9) has two conjugate complex roots, denoted as $\lambda_{1,2} = \pm i\omega$ along with a single non-zero real root $\lambda_3 = \frac{2b\,d}{b-d}$. Consequently, the first condition of the Hopf bifurcation theorem is satisfied. It should be noted that, in general, $\lambda = \lambda(a)$. Using equation (9), the relationship can be established as follows:

$$f(\lambda(a),a) = \lambda^3(a) + (a-b+d)\lambda^2(a) + a(d-b)\lambda(a) + 2abd.$$

The root $\lambda = \lambda(a)$ of equation (9) satisfies the condition

$$f(\lambda(a),a) = 0. \tag{10}$$

Taking the derivative of equation (10) with respect to a yields

$$\frac{\partial f}{\partial \lambda(a)}\frac{d\lambda(a)}{da} + \frac{\partial f}{\partial a} = 0$$

which implies that

$$\frac{d\lambda(a)}{da} = \frac{\lambda^2(a)+(d-b)\lambda(a)+2bd}{-3\lambda^2(a)-2(a-b+d)\lambda(a)+a(b-d)}\ . \tag{11}$$

By taking the root $\lambda(a) = \lambda_{1,2}(a)$ and evaluating it at $a = a^*$, where $\lambda_{1,2}(a) = \pm i\omega$, the value of λ_1 can be substituted into equation (11), leading to the result

$$\frac{d}{da}\mathrm{Re}\left(\lambda_{1,2}(a)\right)|_{a=a^*} = \alpha = \frac{\omega^2(b-d)^2}{2\sigma_1} \neq 0.$$

Thus, the second condition for a Hopf bifurcation is satisfied. Consequently, at E_1, it is concluded that system (3) undergoes a Hopf bifurcation when $a = a^*$, resulting in the appearance of periodic solutions near the equilibrium point. □

We now take a closer look at the Hopf bifurcation in system (3), focusing on the stability of the periodic solutions that emerge after the bifurcation. To assess their stability, we used the first Lyapunov coefficient. To begin the analysis, we shift the equilibrium point E_1 of system (3) to the origin $E_{10} = (0.0.0)$ by applying a linear transformation: $(x,y,z) \mapsto \left(x + x_0, y + \sqrt{x_0}, z + \frac{b}{c}\sqrt{x_0}\right)$. After this change, system (3) takes the following form:

$$\begin{aligned} \dot{x} &= a\left(-x + 2\sqrt{x_0}\,y + y^2\right), \\ \dot{y} &= b\,y - c\,z, \\ \dot{z} &= g\sqrt{x_0}\,x + \frac{bd}{c}\,y - d\,z + g\,x_1x_2, \end{aligned} \tag{12}$$

Now, we need to find the equation that describes the two-dimensional flow on the center manifold at the point where the bifurcation occurs. System (12) has been converted to its canonical form using the following linear transformation.

$$\begin{pmatrix} x \\ y \\ z \end{pmatrix} = T\begin{pmatrix} y_1 \\ y_2 \\ y_3 \end{pmatrix}, \text{ where } T = \begin{pmatrix} \frac{c\omega^2}{b^2 d}\sqrt{x_0} & \frac{-c\omega(b-d)}{b^2 d}\sqrt{x_0} & 1 \\ \frac{c}{b} & 0 & \frac{cg(b-d)^2}{-2bd\omega^2}\sqrt{x_0} \\ 1 & \frac{\omega}{b} & \frac{g(b-d)(b-3d)}{-2d\omega^2}\sqrt{x_0} \end{pmatrix}.$$

We can rewrite system (12) in the following form:

$$\begin{pmatrix} \dot{y_1} \\ \dot{y_2} \\ \dot{y_3} \end{pmatrix} = \begin{pmatrix} 0 & -\omega & 0 \\ \omega & 0 & 0 \\ 0 & 0 & \frac{2bd}{b-d} \end{pmatrix}\begin{pmatrix} y_1 \\ y_2 \\ y_3 \end{pmatrix} + \begin{pmatrix} G_1(y_1,y_2,y_3) \\ G_2(y_1,y_2,y_3) \\ G_3(y_1,y_2,y_3) \end{pmatrix}, \quad (13)$$

where $G_i(y_1,y_2,y_3),\ i=1,2,3$ are defined as follows:

$$\begin{aligned} G_1(y_1,y_2,y_3) = {} & \frac{-c^2 g\omega^2(b-d)(b^2-3\,bd+d^2)}{b^2 d\sigma_1}\sqrt{x_0}y_1^2 + \frac{c^2 g\omega(b-d)^4}{b^2 d\sigma_1}\sqrt{x_0}y_1y_2 \\ & + \frac{cg(b-d)^3(b^2-6\,bd+d^2)}{2bd\sigma_1}y_1y_3 - \frac{cg(b-d)^6}{2bd\omega\sigma_1}y_2y_3 + \frac{3cg^2(b-d)^5}{4d\omega^2\sigma_1}\sqrt{x_0}y_3^2, \\ G_2(y_1,y_2,y_3) = {} & \frac{c^2 g\omega^2\sigma_2}{b^2 d\omega\sigma_1}\sqrt{x_0}y_1^2 + \frac{c^2 g\omega^2(b-d)(b^2+d^2)}{b^2 d\sigma_1}\sqrt{x_0}y_1y_2 \\ & - \frac{cg\sigma_3}{2bd\omega\sigma_1}y_1y_3 - \frac{cg(b-d)^3(b^2+d^2)}{2bd\sigma_1}y_2y_3 - \frac{cg^2(b-d)^2\sigma_4}{2d\omega^3\sigma_1}\sqrt{x_0}y_3^2, \\ G_3(y_1,y_2,y_3) = {} & \frac{-2c^2\omega^4(b^2-3\,bd+d^2)}{b^2(b-d)\sigma_1}y_1^2 + \frac{2c^2\omega^3(b-d)^2}{b^2\sigma_1}y_1y_2 \\ & + \frac{c^2 g\omega^2(b-d)(b^2-6\,bd+d^2)}{b^2 d\sigma_1}\sqrt{x_0}y_1y_3 - \frac{c^2 g\omega(b-d)^4}{b^2 d\sigma_1}\sqrt{x_0}y_2y_3 \\ & + \frac{3cg(b-d)^3}{2\sigma_1}y_3^2, \end{aligned}$$

where $\sigma_2 = b^4 - 4b^3 d - 4bd^3 + d^4$, $\sigma_3 = b^6 - 8\,b^5 d + 15\,b^4 d^2 - 8\,b^3 d^3 + 15\,b^2 d^4 - 8\,bd^5 + d^6$ and $\sigma_4 = b^4 - 3b^3 d - 3bd^3 + d^4$.

According to the center manifold theorem, there is a number $\delta > 0$ and a function H defined near the origin in the neighborhood $N_\delta(0)$, which describes the local center manifold.

$$W^c(0) = \{(y_1,y_2,y_3): y_3 = H(y_1,y_2) \text{ for } \|(y_1,y_2)\| < \delta\}.$$

to find the center manifold of system (13), the following expression is suggested

$$H(y_1,y_2) = \epsilon_1 y_1^2 + \epsilon_2 y_1 y_2 + \epsilon_3 y_2^2 + O(3), \quad (14)$$

where $O(3)$ means terms of orders $y_1^3,\ y_1^2 y_2,\ y_1 y_2^2$ and y_2^3. The coefficients ϵ_1, ϵ_2 and ϵ_3 are found by using the following steps in the derivation

$$\dot{y_3} = \frac{\partial H}{\partial y_1}\dot{y_1} + \frac{\partial H}{\partial y_2}\dot{y_2}. \quad (15)$$

We find the partial derivatives of H and substitute them, along with $\dot{y_1}, \dot{y_2}$ and $\dot{y_3}$ from system (13) in (15). After solving the resulting system, we obtain:

$$\epsilon_1 = \frac{c^2\sigma_5}{2b^3 d\sigma_1\sigma_6},\ \epsilon_2 = \frac{c^2\omega\sigma_7}{b^2\sigma_8} \text{ and } \epsilon_3 = -\frac{c^2\omega^2(b-d)}{2b^3 d\sigma_8}$$

where $\sigma_5 = b^{10} - 16\,b^9 d + 105\,b^8 d^2 - 366\,b^7 d^3 + 742\,b^6 d^4 - 924\,b^5 d^5 + 742\,b^4 d^6 - 366\,b^3 d^7 + 105\,b^2 d^8 - 16\,bd^9 + d^{10}$, $\sigma_6 = b^4 - 6\,b^3 d + 9\,b^2 d^2 - 6\,bd^3 + d^4 \neq 0$, $\sigma_7 = b^7 - 13\,b^6 d + 61\,b^5 d^2 -$

$129\,b^4d^3 + 129\,b^3d^4 - 61\,b^2d^5 + 13\,bd^6 - d^7$ and $\sigma_8 = b^8 - 12\,b^7d + 51\,b^6d^2 - 102\,b^5d^3 + 128\,b^4d^4 - 102\,b^3d^5 + 51\,b^2d^6 - 12\,bd^7 + d^8 \neq 0$.

The dynamics on the centre manifold is described by the following system of differential equations,

$$\begin{pmatrix}\dot{y_1}\\ \dot{y_2}\end{pmatrix} = \begin{pmatrix}0 & -\omega\\ \omega & 0\end{pmatrix}\begin{pmatrix}y_1\\ y_2\end{pmatrix} + \begin{pmatrix}F^1(y_1,y_2)\\ F^2(y_1,y_2)\end{pmatrix} \tag{16}$$

where

$$F^1(y_1,y_2) = \phi_1 y_1^2 + \phi_2 y_1y_2 + \phi_3 y_1^3 + \phi_4 y_1^2y_2 + \phi_5 y_1y_2^2 + \phi_6 y_2^3 + O(4),$$
$$F^2(y_1,y_2) = \varphi_1 y_1^2 + \varphi_2 y_1y_2 + \varphi_3 y_1^3 + \varphi_4 y_1^2y_2 + \varphi_5 y_1y_2^2 + \varphi_6 y_2^3 + O(4),$$

where $O(4)$ means terms of orders $y_1^4,\ y_1^3y_2,\ y_1^2y_2^2,\ y_1y_2^3$ and y_2^4, while ϕ_i and φ_i, $i = 1,\dots,6$ are defined as follows:

$\phi_1 = \frac{c^2g\omega^2(d-b)(b^2-3\,bd+d^2)}{b^2d\sigma_1}\sqrt{x_0}$, $\phi_2 = \frac{gc^2\omega(b-d)^4}{b^2d\sigma_1}\sqrt{x_0}$,

$\phi_3 = \frac{gc^3\omega^4(b^2-6bd+d^2)(b^6-8\,b^5d+23\,b^4d^2-30\,b^3d^3+23\,b^2d^4-8\,bd^5+d^6)(b-d)^3}{4d^2b^4\sigma_1^2\sigma_6}$,

$\phi_4 = \frac{-gc^3\omega^3(b^8-8\,b^7d+12\,b^6d^2+46\,b^5d^3-118\,b^4d^4+46\,b^3d^5+12\,d^6b^2-8\,d^7b+d^8)(b-d)^4}{4b^4d^2\sigma_6\sigma_1^2}$,

$\phi_5 = \frac{-gc^3\omega^2(b^4-8\,b^3d+16\,b^2d^2-8\,bd^3+d^4)(b^4-12\,b^3d+30\,b^2d^2-12\,bd^3+d^4)(b-d)^5}{4d^2b^4\sigma_6\sigma_1^2}$,

$\phi_6 = \frac{-gc^3\omega^3(b^4-8\,b^3d+16\,b^2d^2-8\,bd^3+d^4)(b-d)^8}{4d^2b^4\sigma_6\sigma_1^2}$,

$\varphi_1 = \frac{\omega(b^4-4\,b^3d-4\,bd^3+d^4)c^2g}{b^2d\sigma_1}\sqrt{x_0}$, $\varphi_2 = \frac{\omega^2c^2g(b-d)(b^2+d^2)}{d\sigma_1b^2}\sqrt{x_0}$,

$\varphi_3 = \frac{-c^3g\omega^3(b^6-8\,b^5d+15\,b^4d^2-8\,b^3d^3+15\,b^2d^4-8\,bd^5+d^6)(b^6-8\,b^5d+23\,b^4d^2-30\,b^3d^3+23\,b^2d^4-8\,bd^5+d^6)}{4d^2b^4\sigma_6\sigma_1^2}$,

$\varphi_4 = \frac{\omega^2c^3g(b-d)(b^{12}-12\,b^{11}d+50\,b^{10}d^2-78\,b^9d^3+35\,b^8d^4-78\,b^7d^5+196\,b^6d^6-78\,b^5d^7+35\,b^4d^8-78\,b^3d^9+50\,b^2d^{10}-12\,bd^{11}+d^{12})}{4d^2b^4\sigma_6\sigma_1^2}$,

$\varphi_5 = \frac{-c^3g\omega^3(b^4-8\,b^3d+16\,b^2d^2-8\,bd^3+d^4)(b^6-10\,b^5d+19\,b^4d^2-12\,b^3d^3+19\,b^2d^4-10\,bd^5+d^6)(b-d)^2}{4d^2b^4\sigma_6\sigma_1^2}$,

$\varphi_6 = \frac{\omega^4c^3g(b^2+d^2)(b^4-8\,b^3d+16\,b^2d^2-8\,bd^3+d^4)(b-d)^5}{4d^2b^4\sigma_6\sigma_1^2}$.

A nonlinear change of coordinates is introduced to convert any system with the same structure as system (16) into the following form

$$\begin{pmatrix}\dot{u}\\ \dot{v}\end{pmatrix} = \begin{pmatrix}(l_1u-\beta v)(u^2+v^2)+O(4)\\ (l_1u+\beta v)(u^2+v^2)+O(4)\end{pmatrix}, \tag{17}$$

the polar form as

$$\begin{pmatrix}\dot{r}\\ \dot{\theta}\end{pmatrix} = \begin{pmatrix}l_1r^3+\dots\\ \omega+\beta r^2+\dots\end{pmatrix}. \tag{18}$$

Guckenheimer and Holmes in (Guckenheimer and Holmes, 2013), described the process for calculating the first Lyapunov coefficient $l = l_1(0)$ and provided the corresponding formula.

$$l_1 = \frac{1}{16}\left(K_1 + \frac{K_2}{\omega}\right) \tag{19}$$

where

$$K_1 = F^1_{y_1y_1y_1} + F^1_{y_1y_2y_2} + F^2_{y_1y_1y_2} + F^2_{y_2y_2y_2}.$$
$$K_2 = F^1_{y_1y_2}\left(F^1_{y_1y_1} + F^1_{y_2y_2}\right) - F^2_{y_1y_2}\left(F^2_{y_1y_1} + F^2_{y_2y_2}\right) - F^1_{y_1y_1}F^2_{y_1y_1} + F^1_{y_1y_1}F^2_{y_2y_2}.$$

Therefore,

$$l_1 = \frac{c^3g\ \omega^4(d-b)(3b^4-17b^3d+27b^2d^2-17bd^3+3d^4)}{4\ b^3d\ \sigma_1^2\ \sigma_6}.$$

All the details discussed above regarding the Hopf bifurcation can be summarized in the following theorem.

Theorem 1. *System (3) undergoes a Hopf bifurcation at the equilibrium point E_1 when the parameters $(a,b,c,d,g) \in \Omega_1$ and $\sigma_6\sigma_8 \neq 0$, with the following characteristics:*

- *When the value of $l_1 < 0$, both the equilibrium point E_1 and the periodic solution is stable, indicating that the Hopf bifurcation is supercritical.*
- *When the value of $l_1 > 0$, both the equilibrium point E_1 and the periodic solution is unstable, indicating that the Hopf bifurcation is subcritical.*
- *When $\frac{\alpha}{l_1} > 0$, a periodic solution occurs in the region $a < a^*$. Conversely, when $\frac{\alpha}{l_1} < 0$, a periodic solution occurs in the region $a > a^*$ (Guckenheimer and Holmes, 2013).*

Numerical Example 1. *If we take $b = 1$, $c = 1$, $d = 2$, $g = 2$ and $a = 3$, then $l_1 = -\frac{99}{532} < 0$, $\alpha = -\frac{3}{38} < 0$ and $\omega = \sqrt{3}$. Since $l_1 < 0$, the equilibrium point E_1 is stable, system (3) has a stable periodic solution with a period of $2\sqrt{3}\pi$ and the Hopf bifurcation is of type supercritical. Due to $l_1 < 0$ and $\alpha < 0$, this implies that $\frac{\alpha}{l_1} > 0$. Therefore, this periodic solution occurs for $a < a^* = 3$ (see Fig. 3).*

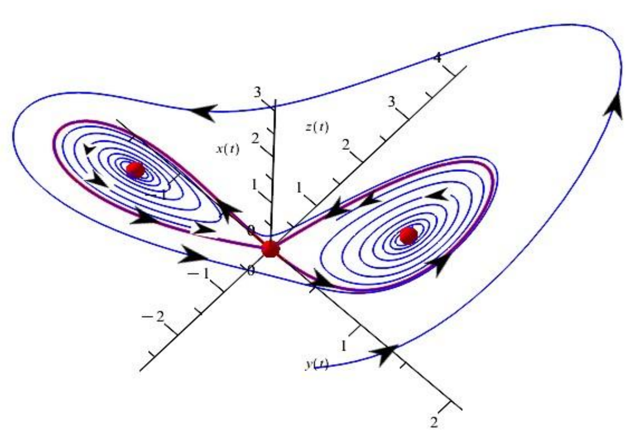

Figure 3: The phase portrait of system (3) is shown when $b = c = 1$ and $a = d = g = 2$. The red balls indicate the equilibrium points, all of which are unstable and the red closed curves indicate the two stable limit cycles.

Numerical Example 2. *Let us consider $b = 2$, $c = 2$, $d = 1$, $g = 1$ and $a = -3$. In this case, it follows that $l_1 = \frac{99}{532} > 0$, $\alpha = -\frac{3}{38} < 0$ and $\omega = \sqrt{3}$. Given that $l_1 > 0$, the equilibrium point E_1 is classified as unstable, it is established that system (3) possesses an unstable periodic solution with a period of $2\sqrt{3}\pi$ and the Hopf bifurcation is of type subcritical. Since $l_1 > 0$ and $\alpha < 0$, it can be inferred that $\frac{\alpha}{l_1} < 0$. Consequently, it is indicated that this periodic solution exists for $a > a^* = -3$ (see Fig. 4).*

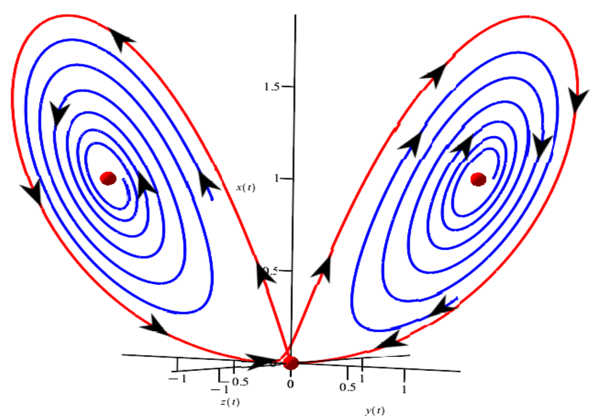

Figure 4: The phase portrait of system (3) is shown when $b = c = 2$, $d = g = 1$ and $a = -2$. The red balls indicate the equilibrium points: the two symmetric points are stable, while the origin is unstable. The red closed curves indicate the two unstable limit cycles.

4 Dynamic Near Infinity

In this section, the behavior of the trajectories of system (3) is investigated near and at infinity by using Poincaré compactification theory in $\mathbb{R}^3$ (Messias et al., 2012, Wang et al., 2014). The polynomial differential system (3), or equivalently, the associated vector field $\chi = (P, Q, R)$, is considered. The degree of χ is defined as $n = \max\{\deg(P, Q, R)\}$.. The Poincaré ball is defined as the unit sphere given by

$\mathbb{S}^3 = \{r = (r_1, r_2, r_3, r_4) \in \mathbb{R}^4 : \| r \| = 1\}$.

Additionally, the sets

$\mathbb{S}_+ = \{r \in \mathbb{S}^3, r_4 > 0\}$ and $\mathbb{S}_- = \{r \in \mathbb{S}^3, r_4 < 0\}$ are identified as the northern and southern hemispheres, respectively. The local charts U_i, V_i for $i = 1,2,3,4$ are used to denote the tangent hyperplanes at the points $(\pm1,0,0,0)$, $(0,\pm1,0,0)$, $(0,0,\pm1,0)$. $(0,0,0,\pm1)$, where $U_i=\{r\in\mathbb{S}^3, r_i>0\}$ and $V_i=\{r\in\mathbb{S}^3,\ r_i<0\}$. The analysis is concentrated on the local charts U_i, V_i for $i=1,2,3$ to derive the dynamics at infinity in the x, y and z directions, respectively.

4.1 The Local Charts U_1 and V_1

The change of variables $(x,y,z)=(w^{-1},uw^{-1},vw^{-1})$ and $t=w\tau$ is applied, transforming system (3) into

$$\begin{aligned}\dot{u}&=-au^3+auw+buw-cvw,\\ \dot{v}&=-au^2v+avw-dvw+gu,\\ \dot{w}&=-a(u^2-w)w,\end{aligned}\tag{20}$$

When $w=0$, system (20) is reduced to

$$\begin{aligned}\dot{u}&=-au^3,\\ \dot{v}&=gu-au^2v,\end{aligned}\tag{21}$$

A line of equilibrium points exists along the v-axis for system (21). Despite this, we can still employ a geometrical approach to analyze the phase portrait by examining the signs of $\dot{u}$ and $\dot{v}$. We obtain two nullclines: one from $\dot{u}=0$, which gives $u=0$ and the other from $\dot{v}=0$, resulting in $v=\frac{g}{a}\frac{1}{u}$ where $a\neq0$. These nullclines partition the plane into four distinct regions. The sign of the ratio $\frac{g}{a}$ is crucial for determining the location of the second nullcline and the direction of the trajectories within these regions. The general directions of the vector field are identified, indicating whether it points upward, downward, to the right, or to the left. Depending on the sign of the parameter ratio, we can observe various trajectories in the local phase portraits, also depicted in Fig. 5. In the local chart V_1, the flow is considered equivalent to that in the local chart U_1, albeit with time reversed. Consequently, the phase portrait of (3) at the sphere at infinity is positioned at the negative endpoint of the x-axis, as illustrated in Fig. 5, again with the time direction reversed.

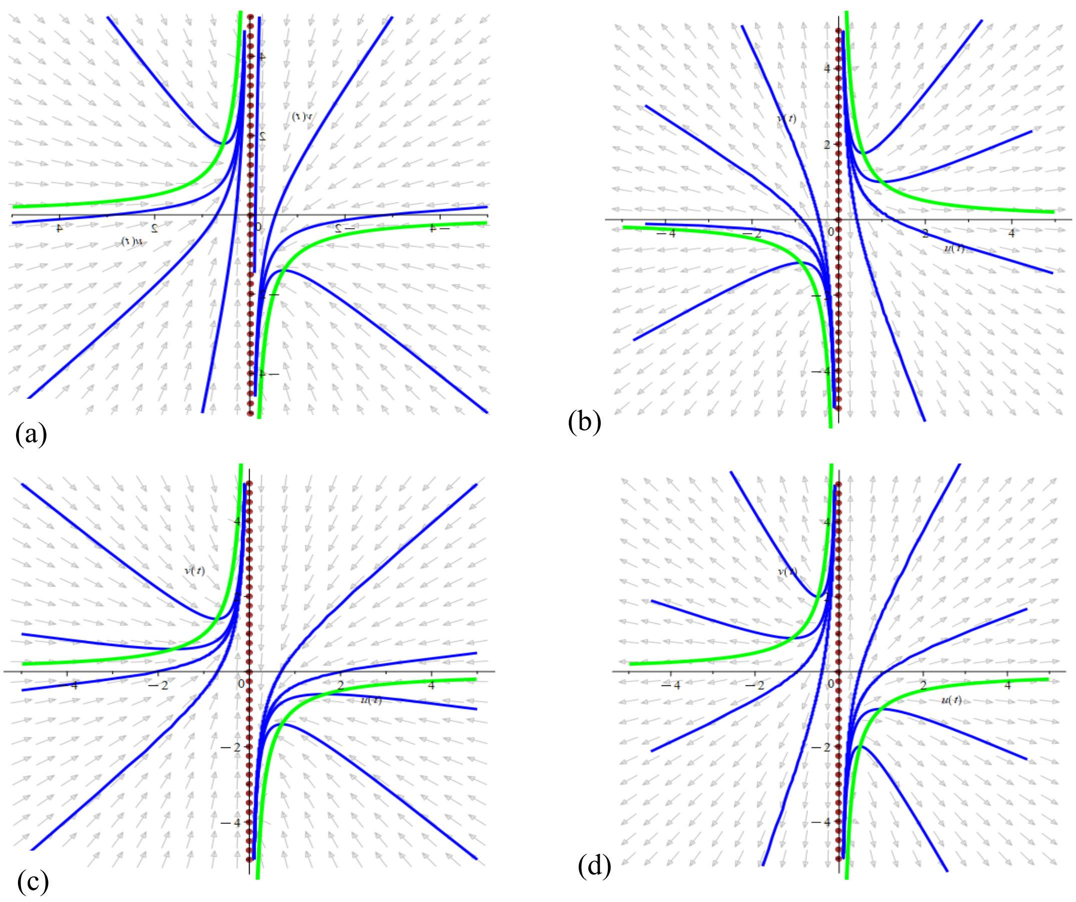

Figure 5: Local phase portraits of system (21) when; **(a)** $a=g=1$. **(b)** $a=g=-1$. **(c)** $a=1$ and $g=-1$. **(d)** $a=-1$ and $g=1$. The green curves, the brown points and the blue curves indicate the nullclines, the line of equilibrium points and the level curves, respectively.

4.2 The Local Charts U_2 and V_2

The dynamics of system (3) are investigated at infinity along the y-axis. By applying the transformation $(x,y,z)=(uw^{-1},w^{-1},vw^{-1})$ with $t=w\tau$, system (3) is transformed into

$$\begin{aligned}\dot{u} &= a+cuvw-auw-buw,\\ \dot{v} &= gu+cv^2w-bvw-dvw,\\ \dot{w} &= -w^2(-cv+b),\end{aligned} \tag{22}$$

When $w=0$, system (22) is reduced to

$$\begin{aligned}\dot{u} &= a,\\ \dot{v} &= gu,\end{aligned} \tag{23}$$

This system has no equilibrium points because $\dot{u}\neq 0$ when $a\neq 0$. The first integral $H(u,v)=v-\frac{g}{2a}u^2$ is present. Moreover, the v-axis serves as a nullcline of the system, dividing the plane into two regions. The signs of the parameters a and g play an important role, as shown in Fig. 6. A geometric approach can be employed to analyze the phase portrait by considering the signs of $\dot{u}$ and $\dot{v}$ alongside information about the first integral and nullclines. The flow in the local chart V_2 is found to correspond to that in the local chart U_2. Thus, the phase portrait of system (3) at the negative infinite endpoint of the y-axis is illustrated in Fig. 6, with the direction of time being reversed.

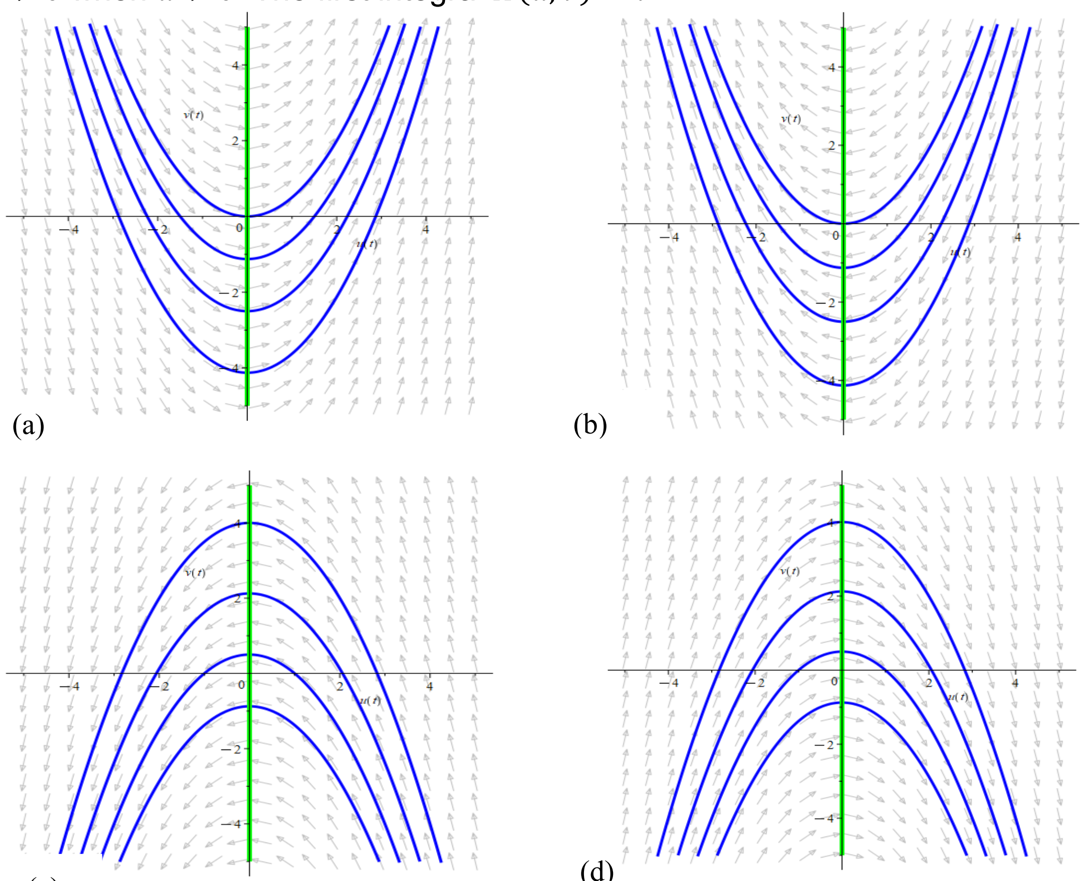

Figure 6: Local phase portraits of system (23) when; **(a)** $a=g=1$. **(b)** $a=g=-1$. **(c)** $a=1$ and $g=-1$. **(d)** $a=-1$ and $g=1$. The green line and the blue curves indicate the nullcline and the level curves, respectively.

4.3 The Local Charts U_3 and V_3

Finally, infinity along the z-axis is examined. By using the transformation $(x,y,z)=(uw^{-1},vw^{-1},w^{-1})$ and $t=w\tau$, system (3) is transformed into:

$$\begin{aligned} \dot{u} &= -gu^2v-auw+av^2+duw,\\ \dot{v} &= -cw-guv^2+bvw+dvw, \\ \dot{w} &= (-guv+dw)w, \end{aligned} \quad (24)$$

When $w=0$, system (24) is simplified to

$$\begin{aligned} \dot{u} &= -gu^2v+av^2,\\ \dot{v} &= -guv^2, \end{aligned} \quad (25)$$

which has a line of equilibrium points located on the u-axis. The equilibrium point at the origin is determined to be unstable. However, a geometrical approach can still be employed to determine the phase portrait by considering the signs of $\dot{u}$ and $\dot{v}$. When $\dot{u}=0$ and $\dot{v}=0$, three nullclines are obtained, which are $u=0$, $v=0$ and $v=\frac{g}{a}u^2$ (with $a\neq 0$). These nullclines divide the plane into six regions, as shown in Fig. 7. The sign of the ratio a and g is relevant in determining the direction of the trajectories. The general directions of the vector field in these regions can also be found, indicating whether the vector field points upward, downward, to the right, or to the left. Some trajectories in the local phase portraits can be obtained, as depicted in Fig. 7, depending on the sign of the ratio of the parameters. The flow in the local chart V_3 is considered to be the same as that in the local chart U_3, with the time being reversed. Hence, the phase portrait of system (3) at infinity is located at the negative endpoint of the z-axis, as shown in Fig. 7, with the direction of time being reversed.

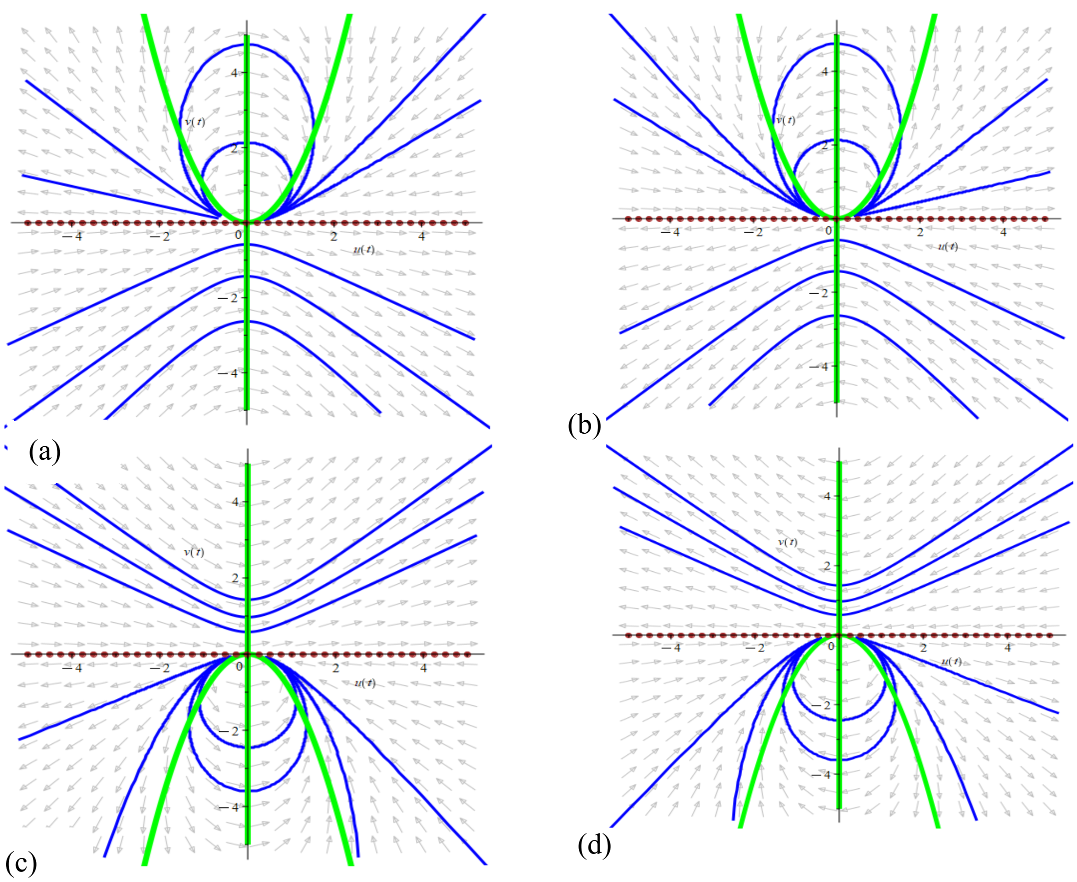

Figure 7: Local phase portraits of system (25) when; **(a)** $a=g=1$. **(b)** $a=g=-1$. **(c)** $a=1$ and $g=-1$. **(d)** $a=-1$ and $g=1$. The green line (curvies) and the blue curves indicate the nullcline and the level curves, respectively.

From the above analysis, the following proposition is presented.

Proposition 4. *For any values of the parameters b, c and d, depending on the signs of a and g, the phase portrait of system (3) is illustrated on the Poincaré sphere at infinity in Fig. 8. Four unstable equilibrium points are located at the positive and negative ends of the x and z axes, with no equilibrium point at the positive and negative ends of the y axis.*

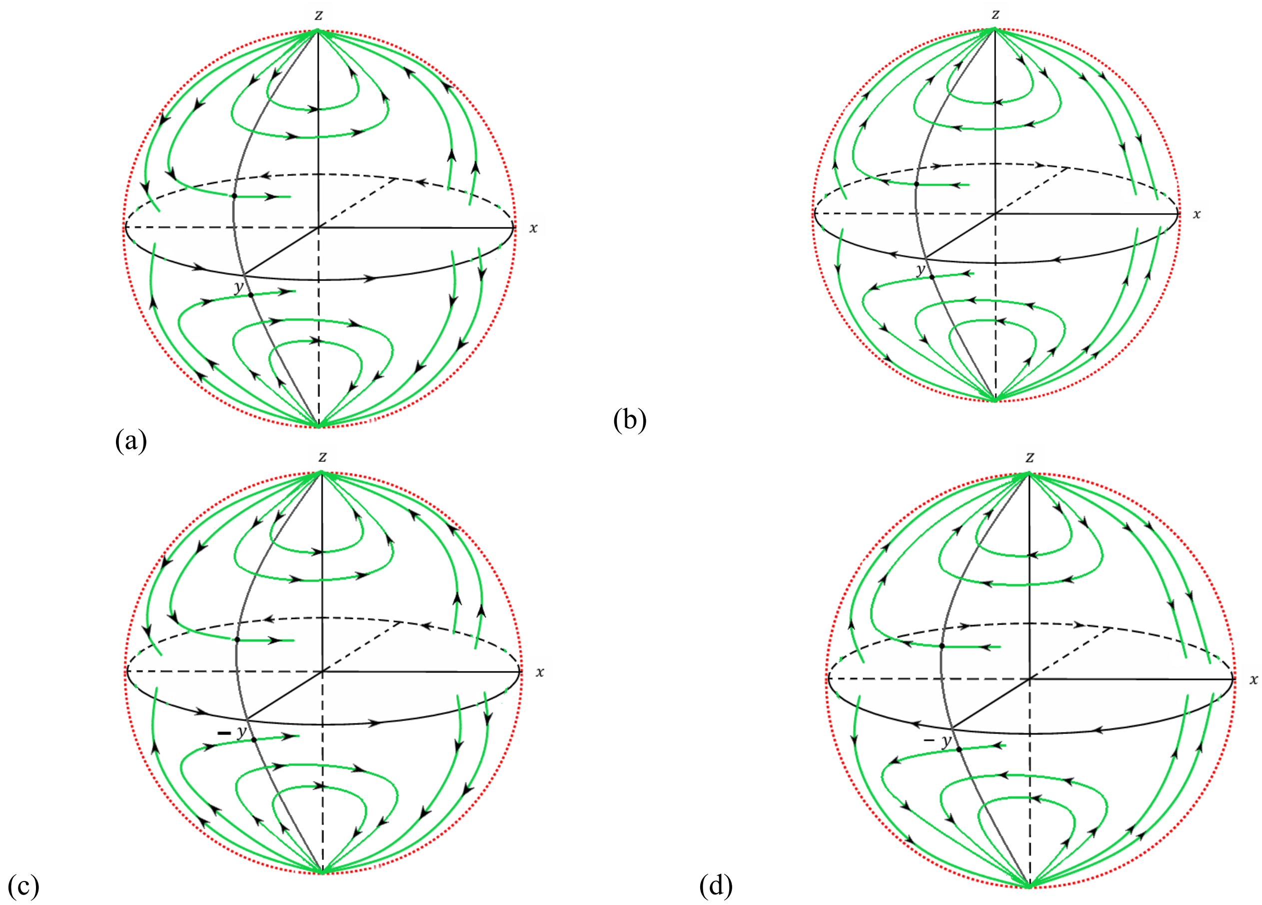

Figure 8: Phase portrait of system (3) on the Poincaré sphere at infinity. **(a)** When $a = g = 1$. **(b)** When $a = g = -1$. **(c)** When $a = 1$ and $g = -1$. **(d)** When $a = -1$ and $g = 1$.

5 Conclusions

The dynamics of a modified three-dimensional Lü system are analyzed in this study, with a focus on the stability of its equilibrium points and the occurrence of Hopf bifurcations. The stability of the system's equilibrium points is examined through characteristic equations. It is illustrated that the stability of the system is highly sensitive to parameter values, which determine the nature of the equilibrium points. Specifically, conditions are identified under which Hopf bifurcations occur at the non-origin equilibrium point, leading to the emergence of periodic solutions. It is demonstrated that both stable and unstable periodic orbits can arise from these bifurcations, depending on the parameter settings. Numerical examples are presented to show both stable and unstable periodic solutions. Additionally, the first Lyapunov coefficient is employed to assess the stability of the periodic solutions, confirming the potential for cyclic behavior in the system. To understand the global behavior of the system, dynamics at infinity are studied using Poincaré compactification theory.

Funding: This research received no external funding.

Conflict of Interest: The authors declare no conflict of interest.

6 References

Algaba, A., Domínguez-Moreno, M. C., Merino, M. & Rodríguez-Luis, A. J. 2015. Study of the Hopf bifurcation in the Lorenz, Chen and Lü systems. *Nonlinear Dynamics,* 79**,** 885-902.

Amen, A. I. & Salih, R. H. 2008. Limit cycles of Lorenz system with Hopf bifurcation. *AL-Rafidain Journal of Computer Sciences and Mathematics,* 5**,** 81-99.

Arrowsmith, D. K. & Place, C. M. 1982. Ordinary Differential Equations: A qualitative approach with applications. *(No Title)*.

Blé, G., Castellanos, V. & Llibre, J. 2016. Existence of limit cycles in a tritrophic food chain model with Holling functional responses of type II and III. *Mathematical Methods in the Applied Sciences,* 39**,** 3996-4006.

Buică, A., García, I. A. & Maza, S. 2012. Existence of inverse Jacobi multipliers around Hopf points in R3: emphasis on the center problem. *Journal of Differential Equations,* 252**,** 6324-6336.

Chen, G. & Dong, X. 1998. *From chaos to order: methodologies, perspectives and applications*, World Scientific.

Chen, G. & Ueta, T. 1999. Yet another chaotic attractor. *International Journal of Bifurcation and chaos,* 9**,** 1465-1466.

Dias, F. S. & Mello, L. F. 2013. Hopf bifurcations and small amplitude limit cycles in Rucklidge systems. *Electron. J. Differ. Equ,* 48**,** 1-9.

Guckenheimer, J. & Holmes, P. 2013. *Nonlinear oscillations, dynamical systems, and bifurcations of vector fields*, Springer Science & Business Media.

Guo, G., Wang, J. & Wei, M. 2023. Stability and Hopf bifurcation in the general Langford system. *Qualitative theory of dynamical systems,* 22**,** 144.

Huang, G. & Cao, Z. 2014. Numerical analysis and circuit realization of the modified LÜ chaotic system. *Systems Science & Control Engineering: An Open Access Journal,* 2**,** 74-79.

Husien, A. M. & Amen, A. I. 2024. Hopf and zero-Hopf bifurcation analysis for a chaotic system. *International Journal of Bifurcation and Chaos,* 34**,** 2450104.

Jiang, J. & Wu, Q. 2016. A New Three-Dimensional Chaotic System with Constant Exponent Spectrum: Analysis, Synchronization and Circuit Implementation. *J. Softw.,* 11**,** 494-511.

Llibre, J. & Pessoa, C. 2015. The Hopf bifurcation in the Shimizu–Morioka system. *Nonlinear Dynamics,* 79**,** 2197-2205.

Lorenz, E. 1963. J. of Atmos. *Sci,* 20**,** 130.

Lorenz, E. N. 2017. Deterministic nonperiodic flow 1. *Universality in Chaos, 2nd edition.* Routledge.

Lü, J. & Chen, G. 2002. A new chaotic attractor coined. *International Journal of Bifurcation and chaos,* 12**,** 659-661.

Lü, J., Chen, G. & Zhang, S. 2002a. Dynamical analysis of a new chaotic attractor. *International Journal of Bifurcation and chaos,* 12**,** 1001-1015.

Lü, J., Lu, J.-A. & Chen, S.-H. 2002b. Chaotic time series analysis and its applications. *Wuhan: Wuhan University Publication*.

Mello, L. F. & Coelho, S. F. 2009. Degenerate Hopf bifurcations in the Lü system. *Physics Letters A,* 373**,** 1116-1120.

Messias, M., Gouveia, M. R. A. & Pessoa, C. 2012. Dynamics at infinity and other global dynamical aspects of Shimizu–Morioka equations. *Nonlinear Dynamics,* 69**,** 577-587.

Mikaeel, S. H., Salih, R. H. & Ahmad, I. 2025. On the Dynamics of a Hyperjerk System and Its Reduction to the Generalized Michelson System. *International Journal of Bifurcation and Chaos***,** 2550161.

Mohammed, B. M. 2025. Hopf Bifurcation in a Novel 3D-Chaotic System with a Four-Wing Attractor. *International Journal of Bifurcation and Chaos,* 35**,** 2530011.

Mohammed, R. H. S. B. M. 2024. Stability and Hopf bifurcation in a modified Sprott C system. *Tatra Mt. Math. Publ,* 88**,** 59-72.

Rasul, T. I. & Salih, R. H. 2024. Hopf bifurcation of three-dimensional quadratic jerk system. *Baghdad Science Journal,* 21**,** 2378-2378.

Salih, H. 2011. The stability analysis of the shimizu-morioka system with Hopf bifurcation. *Journal of Kirkuk University-Scientific Studies,* 6**,** 184-200.

Salih, R. H. 2015. Hopf bifurcation and centre bifurcation in three dimensional Lotka-Volterra systems.

Salih, R. H. & Hasso, M. S. 2017. Centre bifurcations of periodic orbits for some special three dimensional systems. *Electronic Journal of Qualitative Theory of Differential Equations***,** 1-10.

Salih, R. H. & Mohammed, B. M. 2022. Hopf bifurcation analysis of a chaotic system. *Zanco Journal of Pure and Applied Sciences,* 34**,** 87-100.

Sang, B. 2021. Focus quantities with applications to some finite-dimensional systems. *Mathematical Methods in the Applied Sciences,* 44**,** 464-475.

Sang, B. & Huang, B. 2017. Bautin bifurcations of a financial system. *Electron. J. Qual. Theory Differ. Equ,* 2017**,** 1-22.

Sarmah, H. K., Das, M. C. & Baishya, T. K. 2015. Hopf bifurcation in a chemical model. *International Journal for Innovative Research in Science and Technology,* 1**,** 23-33.

Sotomayor, J., Mello, L. F. & Braga, D. D. C. 2006. Stability and Hopf bifurcation in the Watt governor system. *arXiv preprint math/0604177*.

Sotomayor, J., Mello, L. F. & Braga, D. D. C. 2007. Bifurcation analysis of the Watt governor system. *Computational & Applied Mathematics,* 26**,** 19-44.

Strogatz, S. H. 2024. *Nonlinear dynamics and chaos: with applications to physics, biology, chemistry, and engineering*, Chapman and Hall/CRC.

Sun, M., Tian, L. & Yin, J. 2006. Hopf bifurcation analysis of the energy resource chaotic system. *International Journal of Nonlinear Science,* 1**,** 49-53.

Ueta, T. & Chen, G. 2000. Bifurcation analysis of Chen's equation. *International Journal of Bifurcation and Chaos,* 10**,** 1917-1931.

Van Gorder, R. A. & Choudhury, S. R. 2011. Analytical Hopf bifurcation and stability analysis of T system. *Communications in Theoretical Physics,* 55**,** 609.

Vaněček, A. & Čelikovský, S. 1996. *Control systems: from* *linear analysis to synthesis of chaos*, Prentice Hall International (UK) Ltd.

Wang, G., Zhang, X., Zheng, Y. & Li, Y. 2006. A new modified hyperchaotic Lü system. *Physica A: Statistical Mechanics and its Applications,* 371**,** 260-272.

Wang, X. 2009. Si'lnikov chaos and Hopf bifurcation analysis of Rucklidge system. *Chaos, Solitons & Fractals,* 42**,** 2208-2217.

Wang, Z., Wei, Z., Xi, X. & Li, Y. 2014. Dynamics of a 3D autonomous quadratic system with an invariant algebraic surface. *Nonlinear Dynamics,* 77**,** 1503-1518.

Wu, R. & Fang, T. 2015. Stability and Hopf bifurcation of a Lorenz-like system. *Applied Mathematics and Computation,* 262**,** 335-343.

Xiao, M. & Cao, J. 2007. Bifurcation analysis and chaos control for Lü system with delayed feedback. *International Journal of Bifurcation and Chaos,* 17**,** 4309-4322.

Yu, Y. & Zhang, S. 2003. Hopf bifurcation in the Lü system. *Chaos, Solitons & Fractals,* 17**,** 901-906.

Yu, Y. & Zhang, S. 2004. Hopf bifurcation analysis of the Lü system. *Chaos, Solitons & Fractals,* 21**,** 1215-1220.